J. Plasma Phys. (2024), *vol*. 90, 905900302
Published by Cambridge University Press

doi:10.1017/S0022377824000576

Towards ion stopping power experiments with the laser-driven LIGHT beamline

H. Nazary [1,†], M. Metternich [2], D. Schumacher [2], F. Neufeld [1], S.J. Grimm [1], C. Brabetz [2], F. Kroll [3,4], F.-E. Brack [3,4], A. Blažević [2,5], U. Schramm [3,4], V. Bagnoud [1,2,5] and M. Roth [1]

[1]Institut für Kernphysik, Technische Universität Darmstadt, Schlossgartenstr. 9, 64289 Darmstadt, Germany

[2]GSI Helmholtzzentrum für Schwerionenforschung GmbH, Planckstr. 1, 64291 Darmstadt, Germany

[3]Helmholtz-Zentrum Dresden-Rossendorf, 01328 Dresden, Germany

[4]TUD Dresden University of Technology, 01062 Dresden, Germany

[5]Helmholtz-Institut Jena, 07734 Jena, Germany

(Received 29 September 2023; revised 9 April 2024; accepted 10 April 2024)

The main emphasis of the Laser Ion Generation, Handling and Transport (LIGHT) beamline at GSI Helmholtzzentrum für Schwerionenforschung GmbH are phase-space manipulations of laser-generated ion beams. In recent years, the LIGHT collaboration has successfully generated and focused intense proton bunches with an energy of 8 MeV and a temporal duration shorter than 1 ns (FWHM). An interesting area of application that exploits the short ion bunch properties of LIGHT is the study of ion-stopping power in plasmas, a key process in inertial confinement fusion for understanding energy deposition in dense plasmas. The most challenging regime is found when the projectile velocity closely approaches the thermal plasma electron velocity ($v_i \approx v_{e,\mathrm{th}}$), for which existing theories show high discrepancies. Since conclusive experimental data are scarce in this regime, we plan to conduct experiments on laser-generated plasma probed with ions generated with LIGHT at a higher temporal resolution than previously achievable. The high temporal resolution is important because the parameters of laser-generated plasmas are changing on the nanosecond time scale. To meet this goal, our recent studies have dealt with ions of lower kinetic energies. In 2021, laser accelerated carbon ions were transported with two solenoids and focused temporally with LIGHT's radio frequency cavity. A bunch length of 1.2 ns (FWHM) at an energy of 0.6 MeV u^{-1} was achieved. In 2022, protons with an energy of 0.6 MeV were transported and temporally compressed to a bunch length of 0.8 ns. The proton beam was used to measure the energy loss in a cold foil. Both the ion and proton beams will also be employed for energy loss measurements in a plasma target.

Keywords: intense particle beams, plasma applications

† Email address for correspondence: h.nazary@gsi.de

1. Introduction

Ion stopping in plasma is an important topic in inertial confinement fusion (ICF) which is researched as a potential source of energy. The energy loss of the 3.5 MeV α-particles produced in deuterium–tritium fusion reactions must dominate all loss processes, causing the target to self-heat, ultimately leading to further fusion reactions. Therefore, modelling the various plasmas within the dynamic environments of a burning fusion pellet is necessary. This is especially true for ignition and the launch of a thermonuclear burn wave, which will ultimately result in an energy gain (Hurricane *et al.* 2016). For target heating schemes using ion beams as the primary drivers, such as heavy-ion fusion (Callahan-Miller & Tabak 2000) or ion-driven fast ignition (Fernandez *et al.* 2014), ion stopping in a plasma is also essential. Theoretical treatment of ion stopping remains a challenging problem despite decades of extensive analytical and numerical studies. The Born approximation and other perturbative theories (Maynard & Deutsch 1985; Peter & Meyer-Ter-Vehn 1991; Li & Petrasso 1993; Deutsch *et al.* 2010) are in good agreement with the data when the projectile ion velocity is much higher than the thermal velocity of the plasma electrons ($v_i \gg v_{e,\mathrm{th}}$) (Dietrich *et al.* 1990; Hoffmann *et al.* 1990; Roth *et al.* 2000; Frank *et al.* 2013; Zylstra *et al.* 2015). The ion stopping at $v_i \leq v_{e,\mathrm{th}}$ is more difficult to describe, but is typically explained by collisional theories that take into account two-body collisions and large-angle scattering between the ions and the plasma electrons. Due to the strong scattering at ion velocities close to $v_{e,\mathrm{th}}$ and significant collective effects, the Born approximation becomes unreliable, and collisional theories fail to provide a thorough, self-consistent understanding of ion stopping. This is attributed to the dynamic dielectric response of the plasma electrons. This coincides with the regime in which the stopping power is at its maximum. Compared with the conventional perturbative models, stopping theories that thoroughly account for coupling effects between projectiles and plasma electrons predict energy losses of 30–50 % less (Gericke & Schlanges 1999, 2003; Brown, Preston & Singleton 2005; Cayzac *et al.* 2015). In ICF, these theoretical uncertainties hinder the precise prediction of α-particle heating, since the condition $v_\alpha \leq v_{e,\mathrm{th}}$ holds for the majority of the time range. In fact, a decreased α-particle stopping causes a nearly equal increase in range. This may have an impact on the thermonuclear burn wave's ignition threshold in the dense main fuel as well as the energy deposition inside the hot spot of a burning deuterium–tritium plasma (Edie *et al.* 2013). By leveraging the advantages of the various approaches used in the various regimes, rigorous quantum mechanical treatments based on convergent kinetic theories attempt to address these issues (Frieman & Book 1963; Kihara *et al.* 1963; Gould & DeWitt 1967; Brown *et al.* 2005); however, it is unclear how to combine them and quantify their errors. Therefore, accurate measurements of the ion stopping near the stopping maximum are crucial for directing theoretical efforts. Although many attempts have been made to theoretically describe the behaviour of ion stopping in high energy density (HED) plasmas (Maynard & Deutsch 1985; Zimmerman 1997; Peter & Meyer-Ter-Vehn 1991; Li & Petrasso 1993; Gericke & Schlanges 1999; Brown *et al.* 2005; Deutsch *et al.* 2010), there is only a small body of experimental evidence to support these theories (Cayzac *et al.* 2017; Chen *et al.* 2018; Frenje *et al.* 2019; Hayes *et al.* 2020; Zylstra *et al.* 2020; Malko *et al.* 2021). This is because suitable laser-generated plasmas in these measurements are typically very small and highly transient, leading to great demands on the equipment of the experimental area and, in particular, on the plasma probing ion beam.

The majority of the experiments mentioned used conventional particle accelerators, similar to that carried out by Cayzac *et al.* (2017) (see figure 1). In this particular

https://doi.org/10.1017/S0022377824000576 Published online by Cambridge University Press

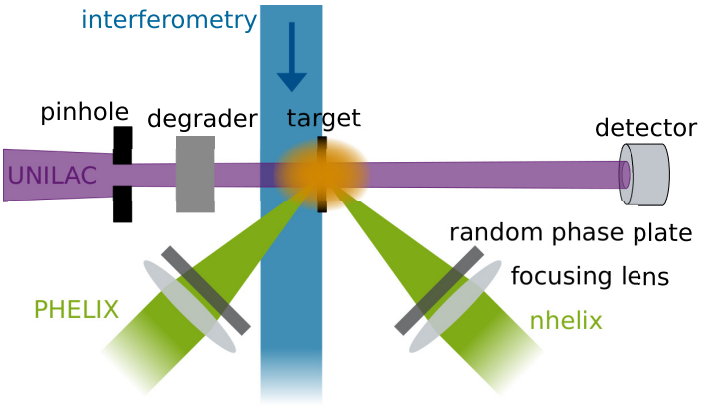

FIGURE 1. Schematic illustration of the previous stopping power experiment conducted by Cayzac *et al.* (2017).

experiment, nitrogen ions were accelerated using the UNIversal Linear ACcelerator (UNILAC) situated at GSI. The ions had an energy of 0.6 MeV u^{-1} and were delivered in bunches lasting $\tau = 5.5$ ns (FWHM) with approximately 1000 ions per bunch. These accelerated ions probed a carbon plasma characterised by free electron densities of up to $n_e = 10^{20}$ cm^{-3} and a maximum temperature of $T_{max} = 150$ eV. Two nanosecond lasers, called Petawatt High Energy Laser for Ion eXperiments (PHELIX) and Nanosecond High Energy Laser for Ion eXperiments (nhelix), generated the plasma. Although the experiment was considered highly successful, the obtained results exhibited significant temporal uncertainties. This can be attributed to the 5.5 ns ion bunch length used in the experiment. As the plasma expands on the nanosecond time scale, its parameters undergo rapid changes, as illustrated in figure 2, displaying simulated temperature profiles at various times during the expansion. Consequently, within the probing ion bunch, leading ions encounter different plasma conditions than trailing ions, causing temporal uncertainties. This issue can be reduced by implementing shorter ion bunches, which can be achieved through the use of laser-generated ions as they have a lower longitudinal emittance (Cowan *et al.* 2004). Another important advantage is the three to four orders of magnitude increase in the number of ions within a probing bunch, resulting in a higher signal-to-noise ratio. This enables an improved measurement accuracy of the stopping power.

Therefore, we intend to expand this experimental dataset by using ions generated by a laser-driven beamline as a probe beam, which have favourable properties compared with ions accelerated by traditional linear accelerators. Intense multi-MeV ion bunches with brief durations can be produced on a μm-scale by laser plasma accelerators. As a result, the characteristics of these laser-generated beams are fundamentally different from those of traditional ion sources, potentially broadening the range of the accelerators' potential for use in research and applications. They can deliver ions with energies above 100 MeV (Kim *et al.* 2016; Wagner *et al.* 2016; Higginson *et al.* 2018; Ziegler *et al.* 2023), in picoseconds at the source (Dromey *et al.* 2016). The target normal sheath acceleration (TNSA) (Wilks *et al.* 2001), which is particularly suitable due to its robustness and the ensuing reliability, is the most researched and frequently used laser-driven ion acceleration mechanism. The

https://doi.org/10.1017/S0022377824000576 Published online by Cambridge University Press

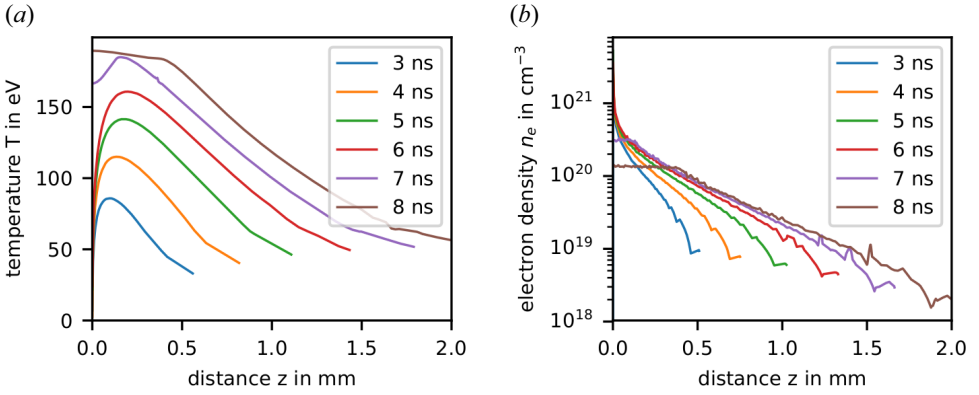

FIGURE 2. Two-dimensional hydrodynamic simulations (MULTI2D Ramis, Meyer-ter Vehn & Ramírez 2009) along the laser axis (z): a carbon foil with a areal density of 100 μg cm^{-2} is irradiated by two lasers beams from both sides (right side of the expansion is shown) with a pulse length of 7 ns (FWHM), a wavelength of 526.5 nm, a focal spot size of 1 mm (supergauss) and an energy of 30 J. (*a*) Simulated plasma temperature at different times of the expansion. (*b*) Simulated free electron density in the plasma at different times of the expansion.

initial TNSA beam is not suitable for the majority of the aforementioned applications due to its broad energy spread, large divergence, and the presence of background radiation in the form of electromagnetic pulses (EMP), X-rays and electrons close to its origin. Using the advantages of laser-driven ions, Malko *et al.* (2021) conducted a successful stopping power experiment with laser-generated protons using magnetic filtering for the energy selection. In numerous laboratories all over the world, a different approach is used to shape the beam to the specific requirements which is the combination of laser-driven beamlines with conventional accelerator components like quadrupoles, solenoids and plasma lenses (Brack *et al.* 2020; Rösch *et al.* 2020; Zhu *et al.* 2020; Apiñaniz *et al.* 2021; Kroll *et al.* 2022).

In this context, the Laser Ion Generation, Handling and Transport (LIGHT) collaboration (Busold *et al.* 2014*a*) was established, and a laser-driven beamline was constructed at GSI. The primary objective of the LIGHT collaboration is to explore the feasibility of working with laser-driven ion beams using traditional accelerator components. Using this understanding, the collaboration aims to maximise bunch intensity and demonstrate the potential of laser-driven beamlines. Due to the preexisting infrastructure at GSI, it is possible to run a radio-frequency (rf) cavity, giving the LIGHT beamline the ability to manipulate the bunches longitudinally and thereby lessen their energy spread or even compress them temporally (Ikegami *et al.* 2009; Busold *et al.* 2013, 2014*b*, 2015; Teng *et al.* 2013; Jahn *et al.* 2019; Metternich *et al.* 2022). The expertise of the Helmholtz-Zentrum Dresden-Rossendorf (HZDR) regarding pulsed high-field solenoid magnets is also advantageous to the LIGHT collaboration. These solenoids have optimised the LIGHT beamline's transverse focusing and capture efficiency.

In this article, we report on the planned stopping power experiment with the LIGHT beamline and the results of two preparatory experimental campaigns in which we demonstrated the generation of the required ion beams and performed a stopping power experiment in a cold foil.

https://doi.org/10.1017/S0022377824000576 Published online by Cambridge University Press

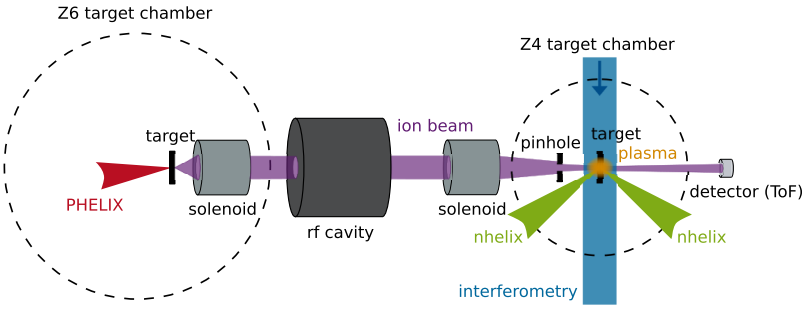

FIGURE 3. Schematic illustration of the planned stopping power experiment with the LIGHT beamline at the Z6 experimental area of GSI.

2. Planned stopping power experiment

In this section, the planned stopping power experiment with the LIGHT beamline will be presented.

The experiment will be performed in the experimental area Z6 at GSI. The set-up of the planned experiment is depicted in figure 3. The objective is to use laser-generated ions with the shortest possible bunch length to investigate their stopping power in a laser-generated plasma. The probed plasma will have a maximum temperature of 150 eV. To achieve the highest ion–plasma coupling in the stopping maximum regime, it is essential to match the velocity of the probing ions with the thermal plasma electrons. This necessitates an energy per mass ratio of 0.5 MeV u^{-1} for the ions. This is a much lower energy per mass than usually targeted at the LIGHT beamline, especially for protons.

The ions are generated and accelerated within the Z6 target chamber via the TNSA mechanism using the PHELIX laser (Bagnoud *et al.* 2010). At the Z6 experimental area, the PHELIX laser's energy is limited to 40 J due to a smaller aperture in the laser beamline. Nevertheless, with a pulse duration of 650 fs (FWHM) and a focal spot size of 3.5 µm (FWHM), the laser intensity exceeds 10^{19} W cm^{-2}, which is sufficient to accelerate ions to MeV energies. Depending on the desired ion species, different targets are employed. The energy spectrum is exponentially decaying and has a cutoff energy of 28.4 MeV for protons (Busold *et al.* 2013). The accelerated ions exhibit high divergence (up to 30° half-opening angle) especially for ions with energies well below the cutoff energy (<1 MeV u^{-1}) which are required for this experiment (Busold 2014). To capture and transport the ions, a high-field solenoid positioned on a hexapod within the Z6 target chamber is used. Placing the first solenoid in close proximity to the TNSA target is essential to enhance its capture efficiency. The casing of the solenoid starts 40 mm behind the TNSA target, to allow a motorised stage with a lens and a mirror to be positioned between the TNSA target and the solenoid before each shot, for the adjustment of the PHELIX laser focus. The solenoid's magnetic field strength is adjusted to select and transport the ions of the desired energy with an energy spread of 20 % through the beamline (Busold *et al.* 2014*b*). The next component in the beamline is the rf cavity. It is a three-gap spiral resonator that is used for longitudinal manipulation of the ion bunch. Due to the low longitudinal emittance of laser-driven ions, it is possible to reduce their energy spread. For protons with an energy of 8 MeV, it was possible to reduce the energy spread from approximately 20 % after the first solenoid to below 3 % (Busold *et al.* 2014*b*, 2015) by accelerating the slow ions in the back of the ion bunch and decelerating the fast ions in the front of the ion bunch with the rf cavity. It is also possible to temporally compress the ion bunch to sub-nanosecond bunch durations (Busold *et al.* 2015; Jahn *et al.* 2019;

https://doi.org/10.1017/S0022377824000576 Published online by Cambridge University Press

Metternich *et al.* 2022) with the same approach by overshooting the energy compression. This results in slower leading ions than trailing ions, which allows the trailing ions to catch up after a certain propagation distance. This methodology will be applied in the stopping power experiment. With this approach, sub-nanosecond ion bunches with an energy spread of 6 % were generated (Metternich *et al.* 2022). Here the rf cavity will be set up to temporally compress the ions at the middle of the second target chamber called Z4, exactly where the plasma target will be positioned. This is done to reduce the temporal uncertainty of the plasma parameters which rapidly change during the expansion. The efficiency of the rf cavity has a minimum at an energy per mass of 0.5 MeV u^{-1}. Therefore, for the stopping power experiment, an energy per mass of 0.6 MeV u^{-1} was targeted. A closer proximity of the rf cavity to the origin of the beam, i.e. the TNSA target, results in the more particles it can temporally compress into the bunch. The minimal distance is limited by the maximum rf cavity voltage and the geometrical constraints at the experimental area Z6 which concludes to a distance of 1225 mm between the TNSA target and the rf cavity. The required cavity voltage for the temporal compression also depends on the distance separating the rf cavity and the plasma target. However, this distance does not have a large effect on the resulting beam parameters. Thus, it is set to 2 m, promoting stable operation of the rf cavity. A second solenoid is used to transversely focus the ion bunch onto the plasma generated in the Z4 target chamber to probe the plasma with as many ions as possible. The optimal placement of the second solenoid depends on the size of the plasma target to be probed by the ion beam. Due to the limited energy of the heating laser (nhelix) and, in turn, the limited focal spot size of 1 mm, the region in which the plasma parameters are spatially homogeneous will only be approximately 0.5 mm in diameter (Cayzac *et al.* 2017). Therefore, the second solenoid must focus the ion beam on the plasma to obtain a sufficient quantity of ions to pass through this region. Since the focal spot size increases with the focal length of the solenoid, the distance of the second solenoid to the plasma target should also be kept as short as possible. Unfortunately, the minimum distance achievable is approximately 1 m, as closer proximity would obstruct the path of the heating laser (see figure 3). Before conducting beamtimes with the LIGHT beamline, simulation studies are performed to predict the resulting beam characteristics and requisite beamline settings. The simulation employs numerical solutions of the Lorentz equation to calculate ion trajectories. For comprehensive information on the workings of the LIGHT beamline simulations, refer to Metternich *et al.* (2022).

To generate the plasma, the nhelix laser is used, as the PHELIX laser is already used to accelerate the ions. For that, the nhelix beam is split into two beams both having an energy of 30 J, a pulse length of 7 ns (FWHM), a wavelength of 527 nm and a focal spot size of 1 mm to achieve plasma parameters similar to those of Cayzac *et al.* (2017). The focus is generated with a random phase plate to achieve an homogeneous spot. The free electron density of the plasma will be measured via interferometry to verify the hydrodynamic simulations of the plasma expansion. These simulations will be used to calculate the stopping power of the ions along the ion path inside the plasma according to the different theoretical models. This is necessary to compare the measurements with the theoretical models. To determine the energy of the ions, a time of flight (ToF) measurement is carried out using an ultrafast diamond membrane detector (Jahn *et al.* 2018). Due to its radiation hardness and high free charge carrier drift mobility, diamond as the active medium of the detector enables a time resolution of tens of picoseconds.

This experiment represents the first of many stopping power experiments using the infrastructure and platform built at the experimental area Z6 at GSI. The LIGHT beamline can cover a wide parameter space for stopping power experiments by employing various configurations of different targets, plasma parameters and ion beams.

https://doi.org/10.1017/S0022377824000576 Published online by Cambridge University Press

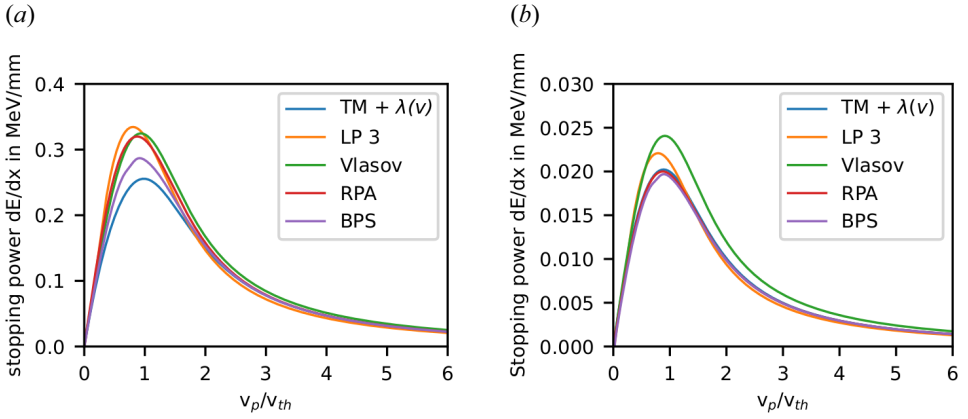

FIGURE 4. Different theoretical models for the stopping of (*a*) carbon ions (C^{4+}) and (*b*) protons plotted over the ratio of the projectile velocity to the thermal velocity of the free electrons in the plasma. TM + $\lambda(v)$ is the T-Matrix formalism with a velocity dependent screening length (Gericke & Schlanges 2003), LP 3 is the Li–Petrasso model (Zylstra *et al.* 2015), Vlasov is the Vlasov model (Peter & Meyer-Ter-Vehn 1991), RPA is the random phase approximation (Zimmerman 1997) and BPS is the Brown Preston Singleton formalism (Brown *et al.* 2005).

It is planned to conduct this experiment for carbon ions and protons as each have certain advantages over the other. Carbon ions experience approximately 13 times higher energy loss in the plasma as can be seen when inspecting the *y*-axis of the plots in figure 4. Additionally, slow carbon ions are also easier to detect with diamond detectors and scintillators since their energy deposition in the detectors is higher. However, protons have only one charge state which means it is unnecessary to estimate their charge state evolution while travelling through the plasma with theoretical models. For carbon ions, the charge state will change within the plasma and theoretical modelling is required. Consequently, using protons makes modelling the experiment easier. Furthermore, the different theoretical models behave differently for different species (see figure 4) particularly in the stopping maximum. This effect can be better evaluated by using both carbon ions and protons in stopping power experiments.

Before conducting such experiments, it is necessary to set up every component and demonstrate its desired functionality. This includes plasma generation with the nhelix laser, which is currently undergoing remodelling to achieve the desired parameters for the experiment. The nhelix laser is scheduled to be completed by December 2023. Additionally, it is important to demonstrate the production of the desired ion beams. To achieve this goal, two preliminary beamtimes were conducted, during which the stopping power in a solid target was measured.

3. Generation of a carbon ion beam

In the following, the results of a preparatory beamtime with carbon ions (C^{4+}) are discussed. As previously mentioned, the goal is to transport carbon ions with an energy of 0.6 MeV u^{-1} to compress them temporally to the shortest possible bunch length and to focus the beam transversely in the centre of the Z4 target chamber. The experimental set-up is identical to that of the planned stopping power experiment with diagnostics placed inside the Z4 target chamber instead of the plasma target.

https://doi.org/10.1017/S0022377824000576 Published online by Cambridge University Press

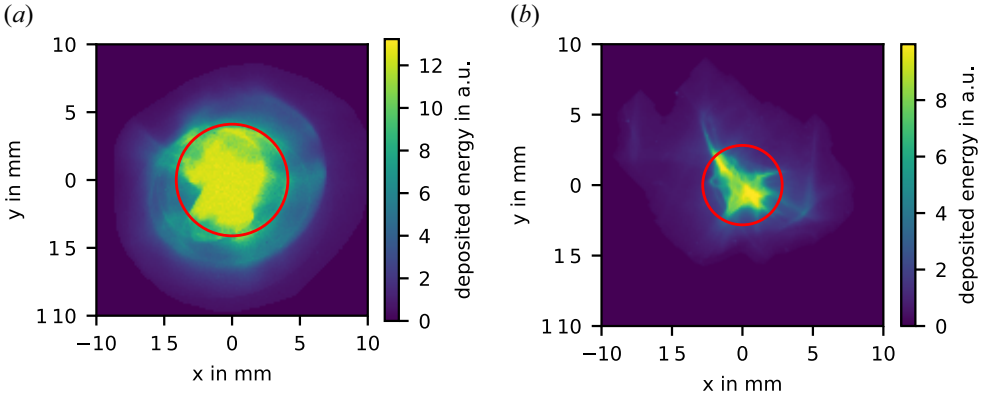

FIGURE 5. Focal spots achieved with the LIGHT beamline of (*a*) carbon ions (C^{4+}) and (*b*) protons measured with radiochromic films in the centre of the Z4 target chamber. Depicted in red is the smallest circle that contains 50 % of the deposited energy.

To accelerate carbon ions, it is necessary to have a target containing carbon atoms and to get rid of the hydrogen contamination on the surface of the target (Hegelich *et al.* 2002). We used a 10 μm thick tungsten foil which had a carbon coating on its rear side with a thickness of 0.9 μm. This target was ohmically heated to temperatures above 1000 °C, resulting in evaporation of the contaminant layer. A pyrometer was used to measure the temperature of the target to ensure that the heating was sufficient and that the target temperature was reached.

To adjust the two solenoids, they were set up to transport protons with an energy of 5.4 MeV, corresponding to the simultaneous transport of C^{4+} ions with an energy of 7.2 MeV (0.6 MeV u^{-1}). Using protons to adjust the beamline eliminates the necessity to heat the target for the adjustment process. The radiochromic film (RCF) measurement in figure 5(*a*) depicts the focal spot of all carbon ions, regardless of their charge state. The achieved focal spot radius, containing 50 % of carbon ions, measured 4.11(2) mm. This is close to the simulated best possible focal spot radius of 3.9 mm, which is limited by the minimal achievable distance between the second solenoid and the focus position.

The next step is to temporally compress the bunch with the rf cavity. For that, an ultrafast diamond membrane detector is used to measure the temporal beam profile of the bunch. The detector is placed in the focal spot which is located in the middle of the Z4 target chamber. A scattering foil (2 μm Mylar) is placed 300 mm in front of the diamond detector to eliminate the transverse filamentation of the beam which is caused by the imperfections in the magnetic field of the solenoid due to its connection cables (Metternich *et al.* 2022). The mean scattering angle is 13 mrad for C^{4+} ions with $E = 7.2$ MeV which corresponds to a location deviation of 3.9 mm over the 300 mm distance according to the Stopping and Range of Ions in Matter code (SRIM Ziegler & Biersack 1985). A photodiode next to the diamond detector is used to measure the electromagnetic radiation from the interaction between the PHELIX laser and the TNSA target. The rising edge of the photodiode can be used to determine the start time of the ions. In figure 6, the temporal shape of the bunch with the rf cavity turned off along with the corresponding time of flight signals of the carbon ions in the simulations is shown. The first peak can be assigned to protons, which means the contamination layer was not completely evaporated from the rear side of the target. The next two peaks from left to right correspond to C^{5+} and C^{4+} ions. The detector shows no signal where the C^{3+} and the C^{2+} ions should arrive. Additionally, the peak at

https://doi.org/10.1017/S0022377824000576 Published online by Cambridge University Press

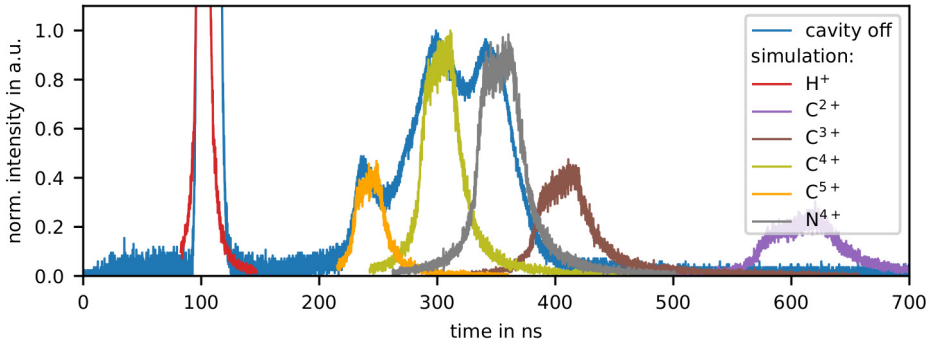

FIGURE 6. Diamond detector signal that corresponds to the time of flight of the ions transported through the LIGHT beamline as well as the time of flight of the transported ions in the simulation. The signals are normalised to the C^{4+} peak.

340 ns could be attributed to N^{4+} ions with $E = 6$ MeV (calculated flight time of 358 ns). Nitrogen, oxygen, hydrogen and carbon are part of the contaminant layer. However, it remains unclear why the low energy ions ($\lesssim 0.4$ MeV u^{-1}) are not detected by the diamond detector. According to SRIM, they are not stopped within the 2 µm thick Mylar foil. Using the Thomson parabola spectra (Ding 2018) and the simulations, we determined that the space charge effects for the C^{3+} are lower than C^{4+} ions, ruling out those effects as the cause of the missing signal. Therefore, we assume that the diamond detector has difficulty detecting ions with low energies ($\lesssim 0.4$ MeV u^{-1}). Nonetheless, the data demonstrate the successful transport of C^{4+} ions with $E = 7.2(2)$ MeV.

For the temporal compression of the C^{4+} ions, the rf cavity voltage and phase were adjusted incrementally. In figure 7, the shortest diamond detector signal (orange) achieved by this procedure is shown along with the signal of the uncompressed beam (blue) and the temporally compressed beam from the simulation (green). It can be seen that not all transported C^{4+} can be compressed to a single bunch, which is due to the long temporal width of the transported C^{4+} within the RF cavity. In this case, the temporal width of the transported C^{4+} within the rf cavity is even longer than twice the period duration which leads to multiple peaks of the C^{4+} at the focal spot in the middle of the Z4 target chamber. The energy transfer from the rf cavity to the ions is velocity dependent due to the three accelerating gaps. This means that other energies are not temporally compressed. For most of the other transported ions, the relative energy transfer is larger, resulting in their temporal compression at a shorter distance. The additional flight distance then leads to a u-shaped temporal profile of the bunch. For the future stopping power experiments, only the temporal compressed carbon ions with an energy of approximately 7.2 MeV are relevant. Since the plasma remains in a relevant state for only 20 ns, it will only affect the desired peak, allowing us to separate the peaks in the measurement. The phase and voltage on each shot are measured to determine the exact cavity settings. In addition, a start detector is used for stopping power experiments to verify the initial energy and ensure accurate measurements. The standard deviation of the measured cavity voltage is 1.23 %, while the measured phase has a standard deviation of 3.1°, equivalent to a 0.08 ns delay. The deviation in voltage affects only the bunch length, whereas the deviation in phase affects both the bunch length and the temporally compressed energy. We simulated a translated standard deviation of 642 eV u^{-1} in energy and 100 ps in pulse length.

https://doi.org/10.1017/S0022377824000576 Published online by Cambridge University Press

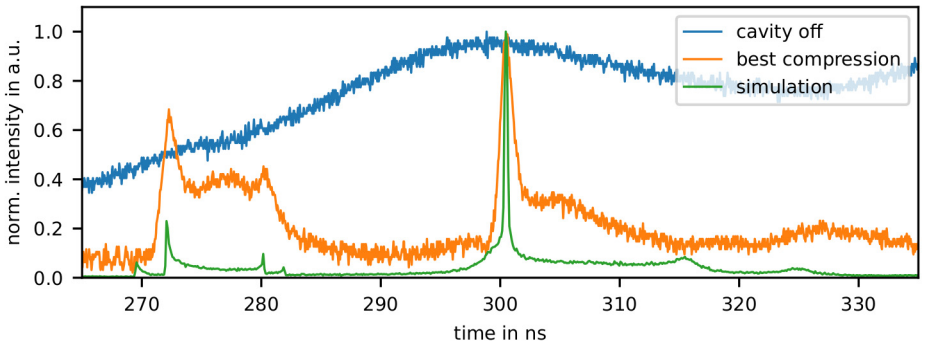

FIGURE 7. Measured and simulated time of flight of the temporally compressed C^{4+} ions along with the measured time of flight of the uncompressed C^{4+} ions.

The flight times and temporal distributions of the various carbon ion bunches exhibit only minor variations. The shortest bunch duration is $\tau = 1.23(4)$ ns (FWHM), which is four times larger than predicted by simulations (see table 1). A range of potential causes, including the scattering foil in ToF measurements, space charge effects, the TNSA-generated ion beam's non-negligible initial emittance and the radial dependency of the electric field within the rf cavity gaps, were thoroughly examined. However, these factors do not appear to explain the observed phenomenon. Saturation effects in the diamond detector could be a plausible cause. This hypothesis requires confirmation through further testing of the diamond detector with lower fluxes and other diagnostics during future beamtimes.

To estimate the number of transported carbon ions, an HD-V2 RCF by Ashland positioned at the location of the diamond detector (see figure 5*a*) measures the deposited energy of the temporally compressed ion beam. The active layer of this RCF has a thickness of 10 μm. During the experiment, the active layer was exposed to the incident beam without any passive layer in front of it. It is assumed that the total energy deposited in the active layer corresponds to the energy of all transported carbon and nitrogen ions. The deposited energy of protons in this layer can be neglected, as those with an energy of 5.25 MeV are not stopped in this layer and lose minimal energy ($\approx$ 8 keV per proton). For the estimation, the energy spectrum of the carbon ions from the simulation was used as the diamond detector faced difficulties in detecting lower energies, rendering it incapable of measuring the spectrum. The transported beam in the simulation, which uses the Thomson parabola spectra measured by Ding (2018) for the TNSA source, comprises 21 % C^{2+}, 26 % C^{3+}, 40 % C^{4+} and 13 % C^{5+} ions. The total energy deposited in the active layer amounts to $E_{\mathrm{dep}} = 2.0(6) \times 10^{10}$ MeV, with the significant uncertainty stemming from a lack of calibration in the used RCF lot, which required us to use a calibration from an older lot. Under the assumption that the spectrum of the measured beam corresponds to the spectrum obtained from simulations, the transported ion beam comprises $3.6(1.1) \times 10^9$ carbon ions, of which $1.4(4) \times 10^9$ are C^{4+} ions. Furthermore, simulations indicate that 14 % of the transported C^{4+} ions can be temporally compressed, equating to $2.0(6) \times 10^8$ temporally compressed C^{4+} ions in the experiment.

In table 1, the most important parameters of the final carbon bunch are summarised and compared with the simulation.

https://doi.org/10.1017/S0022377824000576 Published online by Cambridge University Press

Parameter	Experiment	Simulation
Mean energy	7.2(2) MeV	7.2 MeV
Energy spread (full width of C^{4+} ions)	/	1.94 %
Temporal bunch width (FWHM)	1.23(4) ns	0.3 ns
Focal spot radius (50 % encircled)	4.11(2) mm	3.9 mm
Estimated number of C^{4+} ions	$2.0(6) \times 10^8$	

TABLE 1. Comparison between simulated and measured parameters of the temporally compressed carbon bunch.

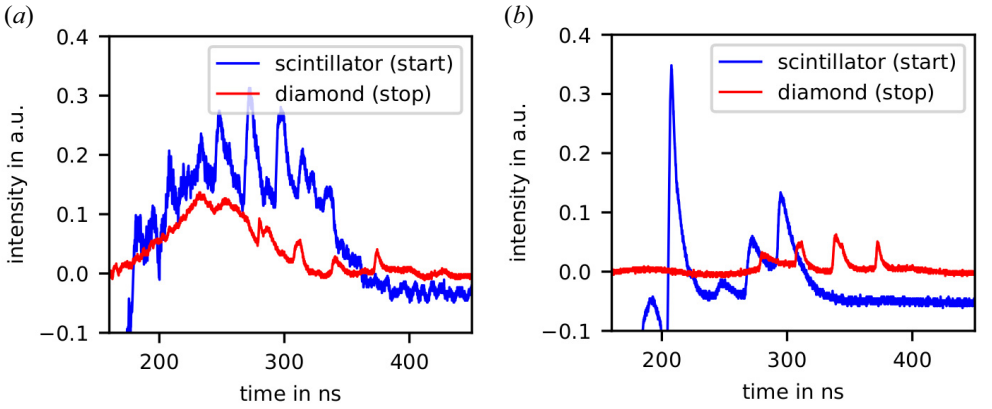

FIGURE 8. Comparison of the signals of a diamond detector used as the stop detector and a scintillator with a photodiode used as the start detector in ToF measurements affected by EMP when using (*a*) a metal target on a metal holder versus (*b*) a plastic target on a plastic holder. The multipeak structure is due to the bunching of the rf cavity.

4. Generation of a proton beam

In this section, the results of the preparatory beamtime for protons are discussed. The goal of this second preparatory beamtime was to transport protons with an energy of 0.6 MeV and to compress them temporally to the shortest possible bunch length. The experimental set-up is identical to the carbon ion beamtime. In addition, simulations were conducted prior to this beamtime.

Heating the target is not required for proton acceleration. A range of TNSA targets was used to determine the most suitable target for the stopping power experiment. Both 10 μm gold and 10 μm tungsten targets were tested, with no observable differences in behaviour. Additionally, we tested 500 nm polystyrene targets, which demonstrated a notable decrease in the electromagnetic pulse (EMP) detected by our time of flight diagnostics. Typically, the targets are mounted on an aluminium holder; we replaced it with a 3-D printed PETG (polyethylene terephthalate glycol-modified) holder. This also significantly reduced the noise caused by the EMP, particularly for the time of flight signal measured with a scintillator (BC-422Q by Saint-Gobain Crystals) and a photodiode (AXUV20HS1 by Optodiode), as demonstrated in figure 8.

https://doi.org/10.1017/S0022377824000576 Published online by Cambridge University Press

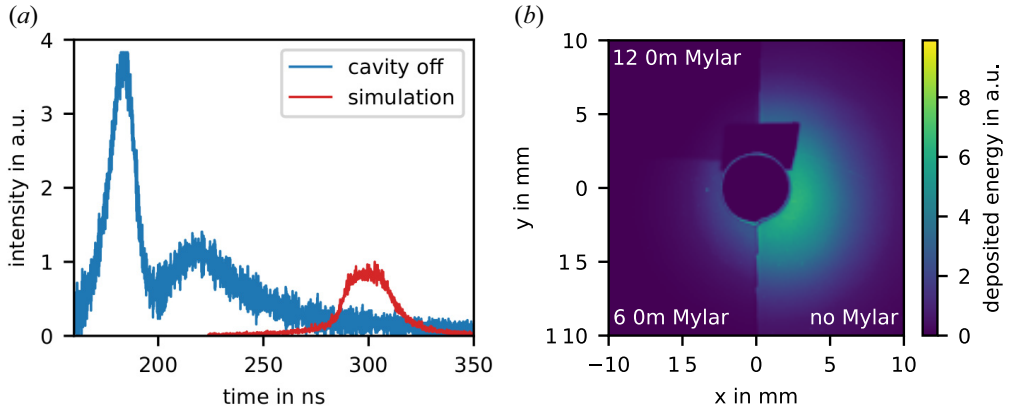

FIGURE 9. (*a*) Diamond detector signal that corresponds to the time of flight of the protons that are transported through the LIGHT beamline as well as the time of flight of the transported protons in the simulation. (*b*) RCF measurement of proton beam with three segments: one with no Mylar foil, one with 6 μm (>0.45 MeV) and one with 12 μm Mylar (>0.7 MeV) in front of it. In the middle of the RCF, there is a hole and a piece of tape.

After adjusting the two solenoids, the achieved focal spot was measured with an RCF and can be seen in figure 5(*b*). A focal spot radius of 2.82(3) mm which contained 50 % of the protons was achieved.

The temporal beam profile of the proton bunch is measured with the ultrafast diamond membrane detector and again a scattering foil was used to disrupt the transverse filamentation of the beam. The signal of the diamond detector is depicted in figure 9(*a*) in conjunction with the simulated proton bunch. The protons with an energy of 0.6 MeV are anticipated to arrive at approximately $t = 295$ ns. It can be seen that the diamond detector had problems detecting the slow protons, thus strengthening the assumption that its efficiency in detecting low-energy particles is questionable. To ensure that the magnets were transporting protons at the correct energy of 0.6 MeV, an RCF measurement was carried out. In front of the active layer of the RCF, Mylar foils of different thicknesses were placed to stop all protons up to a certain energy. Figure 9(*b*) shows the RCF with three segments. The 12 μm Mylar foil stops all protons with an energy lower than 0.7 MeV ($t > 281$ ns), which is a substantial amount, as can be seen. The 6 μm Mylar foil stops all protons with an energy lower than 0.45 MeV ($t > 351$ ns) and in the third segment, all protons lose energy. Since the segment with the 6 μm Mylar foil shows a significant number of protons, we can be sure that protons with an energy between 0.45 MeV and 0.7 MeV (281 ns $< t <$ 351 ns) were transported. In the segment without Mylar, all protons deposit their energy in the active layer. This indicates that, in addition to the targeted proton energies, slower protons are also reaching the end of the beamline. It is evident that these slower protons are not being perfectly transported by solenoids. However, since there are more slower protons in the TNSA spectrum, they exhibit a strong dose on the RCF. Upon turning the rf cavity on, the intensity of the proton bunch with an energy of 0.63(1) MeV increased due to the temporal compression. This consequently enabled detection by the diamond detector. So it was possible to adjust the rf cavity's voltage and phase to reach optimal temporal compression. We achieved the shortest bunch duration of 0.76(4) ns as shown in figure 10 along with the simulated shortest bunch. While the flight times and temporal distributions exhibit minimal deviations, the experimental

https://doi.org/10.1017/S0022377824000576 Published online by Cambridge University Press

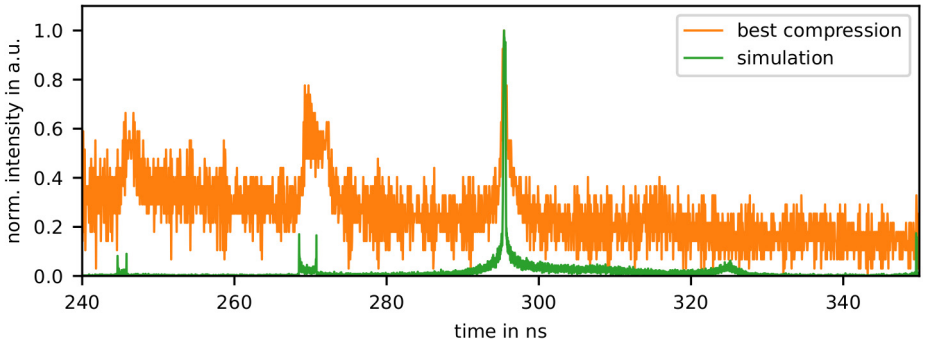

FIGURE 10. Measured and simulated time of flight of the temporally compressed protons.

Parameter	Experiment	Simulation
Mean energy	0.63(1) MeV	0.63 MeV
Energy spread (full width)	/	2.04 %
Temporal bunch width (FWHM)	0.76(4) ns	0.36 ns
Focal spot radius (50 % encircled)	2.82(3) mm	3.9 mm
Estimated number of protons	$5.9(4) \times 10^8$	

TABLE 2. Comparison between simulated and measured parameters of the temporally compressed proton bunch.

bunch duration again exceeds the simulated bunch duration (see table 2) which is likely caused by saturation effects of the diamond detector.

Due to our incomplete understanding of the response of the diamond detector at low energies, we cannot assume that the energy deposited on the RCF is dominated by the protons with an energy of 0.63(1) MeV. Instead, we approximated the number of transported protons by modelling their propagation through the beamline using the proton distribution at the TNSA source, which we measured using radiochromic imaging spectroscopy (RIS) (Schmitz, Metternich & Boine-Frankenheim 2022). This estimation results in $5.8(4) \times 10^8$ temporally compressed protons.

In table 2, the most important parameters of the final proton bunch are summarised and compared with the simulation.

5. Stopping power in cold foil

During the proton beamtime, we conducted an experiment on stopping power using a cold carbon foil which will be reported in this section. For the stopping power experiment, the transported protons passed through a scintillator with a hole in it (see figure 11). This ensured that the protons located on the periphery of the beam were stopped in the scintillator and detected with a photodiode that provided the start signal for the ToF measurement. The scintillator used was a BC-422Q by Saint-Gobain Crystals, and the signal was detected with an AXUV20HS1 photodiode by Optodiode. The protons that passed through the aperture lost energy within the carbon foil located in the focal spot of the proton beam. Following a time of flight distance of $d_{\mathrm{ToF}} = 0.818(2)$ m, a diamond detector with an area of 10×10 mm^2 and with a thickness of 19 µm was employed to

https://doi.org/10.1017/S0022377824000576 Published online by Cambridge University Press

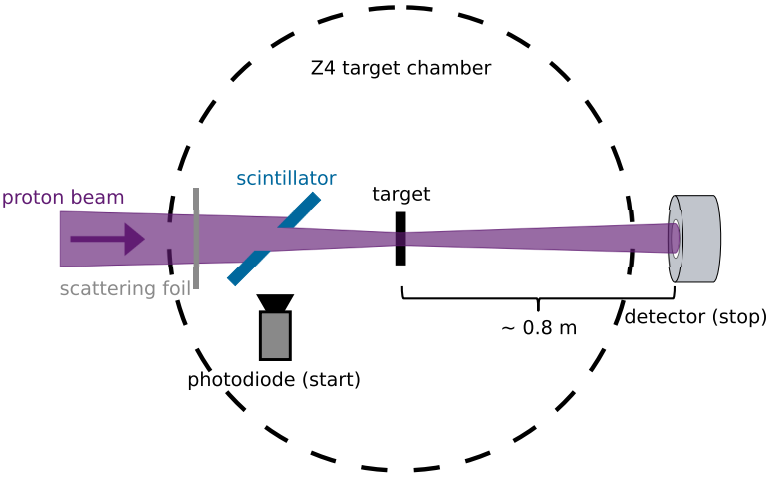

FIGURE 11. Schematic illustration of the stopping power experiment with the LIGHT beamline in a cold carbon foil.

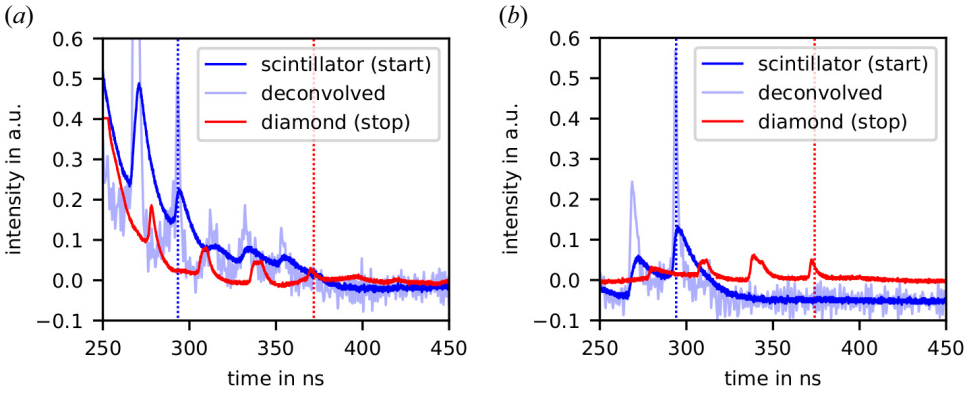

FIGURE 12. Time of flight measurements of the proton energy with a scintillator (start) and a diamond detector (stop). (*a*) Time of flight measurement of initial proton energy without carbon foil. (*b*) Time of flight measurement of final proton energy with carbon foil. The dashed lines show the centre of weight of the protons used for the stopping power measurement.

measure the stop signal. A scattering foil (1 μm thick Mylar) in front of the scintillator was used to disrupt the filamentation of the beam. The stopping target was a carbon foil with an areal density of 105 μg cm^{-2}. Two shots without and two shots with the stopping target were conducted to measure the energy loss of the protons in the carbon foil. Figure 12 illustrates the time signals of the start and stop detectors for a shot without and with the carbon foil.

The signal of the scintillator was deconvolved with the response function of the AXUV photodiode which was measured with a short pulse laser. The response of the scintillator and the diamond detector were not considered since both of them have fast rise and fall times ($\approx 10^{-9}$ s). The shots without the carbon foil are used to measure the initial energy of the proton bunch. The central energy was obtained by using the peaks' centre of weights. An initial energy of $E_i = 595(5)$ keV was determined. The final energy was determined with the two shots in which the protons passed through the carbon foil. The signal was

https://doi.org/10.1017/S0022377824000576 Published online by Cambridge University Press

observed to shift towards later times, indicating a reduction in the energy of the protons. An energy of $E_f = 566(4)$ keV was determined. Using the measured initial energy of the protons, it is possible to calculate their energy after passing through the stopping foil with SRIM, which concludes to $E_{f,\mathrm{SRIM}} = 563(12)$ keV. Since the calculated energy and the measured energy of the protons after passing through the carbon foil are within each other's error bars, we can claim a successful stopping power experiment in a cold foil. We recorded an energy loss of $dE = 29(6)$ keV with an uncertainty of 20 %. According to theoretical models, we anticipate that the protons will lose approximately 70–100 keV in the plasma aimed for in the planned experiment ($E = 2 \times 30$ J, $\lambda = 527$ nm, $\tau = 7$ ns (FWHM), $d = 1$ mm). We expect a reduced uncertainty of approximately 5 keV because the flight time will be longer. For 70 keV, the resulting uncertainty is 7 %. The calculation of stopping power along the ion path, according to theoretical models, will have an uncertainty due to the uncertainty of plasma parameters. The plasma parameters along the ion path are simulated using a hydrodynamic code and verified with interferometric measurements of the free electron density. Based on previous experiments, this uncertainty in calculated energy loss is approximately 10 % (Cayzac *et al.* 2017). This is sufficient to benchmark theoretical models, which show discrepancies of up to 26 % (see figure 4).

6. Conclusion and outlook

In this article, the results of two beamtimes performed as preparation for the planned stopping power experiments in plasma with the LIGHT beamline were presented. They showed the capability of the beamline to generate the required ion beams. Carbon ions (C^{4+}) with an energy of 7.2(2) MeV were successfully transported and temporally compressed to a bunch duration of 1.23(4) ns (FWHM). Also, protons with an energy of 0.63(1) MeV were transported and temporally compressed to a bunch duration of 0.76(4) ns. All the bunch characteristics are summarised in tables 1 and 2. The transported protons were used to perform a stopping power experiment in a solid carbon foil. We measured an energy loss of $dE = 29(6)$ keV, which agrees with the energy loss predicted by SRIM.

The next step is to conduct the planned stopping power experiment with a plasma target. This will allow for theory benchmarking in the regime of the stopping maximum.

Acknowledgements

The authors would like to express their gratitude to the PHELIX laser team for their support, as well as to the HF group of GSI for their assistance. Additionally, the target laboratory at Technische Universität Darmstadt (T. Abel and G. Schaumann) and the target laboratory at GSI are acknowledged for their contributions to target fabrication. The detector laboratory of GSI (M. Träger and M. Kis) is also appreciated for their work on detector development. Finally, the work of the high-field laboratory (HLD) at HZDR for the solenoid construction is also acknowledged. The referees are acknowledged for their valuable comments that have significantly improved the quality of this article.

Editor Per Helander thanks the referees for their advice in evaluating this article.

Declaration of interest

The authors report no conflict of interest.

Data availability

The authors confirm that all of the data and codes used in this study are available from the corresponding author upon reasonable request.

https://doi.org/10.1017/S0022377824000576 Published online by Cambridge University Press

REFERENCES

Apiñaniz, J.I., *et al.* 2021 A quasi-monoenergetic short time duration compact proton source for probing high energy density states of matter. *Sci. Rep*. **11** (1).

Bagnoud, V., *et al.* 2010 Commissioning and early experiments of the PHELIX facility. *Appl. Phys.* B*: Lasers Opt*. **100** (1), 137–150.

Brack, F.E., *et al.* 2020 Spectral and spatial shaping of laser-driven proton beams using a pulsed high-field magnet beamline. *Sci. Rep*. **10** (1).

Brown, L., Preston, D. & Singleton, R. Jr. 2005 Charged particle motion in a highly ionized plasma. *Phys. Rep*. **410** (4), 237–333. arXiv:0501084.

Busold, S. 2014 Construction and characterization of a laser-driven proton beamline at GSI. PhD thesis, Technische Universität Darmstadt.

Busold, S., *et al.* 2014*a* Shaping laser accelerated ions for future applications – The LIGHT collaboration. *Nuclear Instruments and Methods in Physics Research Section A: Accelerators, Spectrometers, Detectors and Associated Equipment* **740**, 94–98.

Busold, S., *et al.* 2015 Towards highest peak intensities for ultra-short MeV-range ion bunches. *Sci. Rep*. **5** (1), 12459.

Busold, S., *et al.* 2013 Focusing and transport of high-intensity multi-MeV proton bunches from a compact laser-driven source. *Phys. Rev. Spec. Top. Accel. Beams* **16** (10).

Busold, S., Schumacher, D., Deppert, O., Brabetz, C., Kroll, F., Blažević, A., Bagnoud, V. & Roth, M. 2014*b* Commissioning of a compact laser-based proton beam line for high intensity bunches around 10 MeV. *Phys. Rev. Spec. Top. Accel. Beams* **17** (3), 031302.

Callahan-Miller, D.A. & Tabak, M. 2000 Progress in target physics and design for heavy ion fusion. *Physics of Plasmas* **7** (5), 2083–2091.

Cayzac, W., *et al.* 2017 Experimental discrimination of ion stopping models near the Bragg peak in highly ionized matter. *Nat. Commun*. **8**, 15693.

Cayzac, W., *et al.* 2015 Predictions for the energy loss of light ions in laser-generated plasmas at low and medium velocities. *Phys. Rev.* E - *Stat. Nonlinear Soft Matt. Phys*. **92** (5), 1–10.

Chen, S.N., *et al.* 2018 Experimental evidence for the enhanced and reduced stopping regimes for protons propagating through hot plasmas. *Sci. Rep*. **8** (1), 1–12.

Cowan, T.E., *et al.* 2004 Ultralow emittance, multi-MeV proton beams from a laser virtual-cathode plasma accelerator. *Phys. Rev. Lett*. **92** (20), 204801.

Deutsch, C., *et al.* 2010 Ion stopping in dense plasma target for high energy density physics. *Open Plasma Phys. J*. **3**.

Dietrich, K.G., Hoffmann, D.H.H., Wahl, H., Haas, C.R., Kunze, H., Brandenburg, W. & Noll, R. 1990 Energy loss of heavy ions in a dense hydrogen plasma. *Z. Phys.* D *Atoms Molec. Clusters* **16** (4).

Ding, J. 2018 Generation, handling and transport of laser-driven heavy ion beams. PhD thesis, Technische Universität Darmstadt.

Dromey, B., *et al.* 2016 Picosecond metrology of laser-driven proton bursts. *Nat. Commun*. **7** (1), 1–6.

Edie, D.J., Vorberger, J., Rose, S. & Gericke, D.O. 2013 α-particle stopping and electron-ion energy relaxation in highly compressed ICF fuel. *EPJ Web of Conferences* **59**, 05018.

Fernandez, J.C., Albright, B.J., Beg, F.N., Foord, M.E., Hegelich, B.M., Honrubia, J.J., Roth, M., Stephens, R.B. & Yin, L. 2014 Fast ignition with laser-driven proton and ion beams. *Nucl. Fusion* **54** (5).

Frank, A., *et al.* 2013 Energy loss and charge transfer of argon in a laser-generated carbon plasma. *Phys. Rev. Lett*. **110** (11).

Frenje, J.A., *et al.* 2019 Experimental validation of low- Z ion-stopping formalisms around the bragg peak in high-energy-density plasmas. *Phys. Rev. Lett*. **122** (1), 1–6.

Frieman, E.A. & Book, D.L. 1963 Convergent classical kinetic equation for a plasma. *Phys. Fluids* **6** (12), 1700–1706.

Gericke, D.O. & Schlanges, M. 1999 Beam-plasma coupling effects on the stopping power of dense plasmas. *Phys. Rev.* E - *Stat. Phys. Plasmas Fluids Relat. Interdiscip. Topics* **60** (1), 904–910.

GERICKE, D.O. & SCHLANGES, M. 2003 Energy deposition of heavy ions in the regime of strong beam-plasma correlations. *Phys. Rev.* E - *Stat. Phys. Plasmas Fluids Relat. Interdiscip. Topics* **67** (3), 4.

GOULD, H.A. & DEWITT, H.E. 1967 Convergent kinetic equation for a classical plasma. *Phys. Rev*. **155** (1), 68–74.

HAYES, A.C., *et al.* 2020 Plasma stopping-power measurements reveal transition from non-degenerate to degenerate plasmas. *Nat. Phys*. **16** (4), 432–437.

HEGELICH, M., *et al.* 2002 MeV ion jets from short-pulse-laser interaction with thin foils. *Phys. Rev. Lett*. **89** (8), 085002/1–085002/4.

HIGGINSON, A., *et al.* 2018 Near-100 MeV protons via a laser-driven transparency-enhanced hybrid acceleration scheme. *Nat. Commun*. **9** (1), 1–9.

HOFFMANN, D.H.H., WEYRICH, K., WAHL, H., GARDÉS, D., BIMBOT, R. & FLEURIER, C. 1990 Energy loss of heavy ions in a plasma target. *Phys. Rev.* A **42** (4).

HURRICANE, O.A., *et al.* 2016 Inertially confined fusion plasmas dominated by alpha-particle self-heating. *Nat. Phys*. **12** (8), 800–806.

IKEGAMI, M., *et al.* 2009 Radial focusing and energy compression of a laser-produced proton beam by a synchronous rf field. *Phys. Rev. Spec. Top. Accel. Beams* **12** (6), 063501.

JAHN, D., *et al.* 2019 Focusing of multi-MeV, subnanosecond proton bunches from a laser-driven source. *Phys. Rev. Accel. Beams* **22** (1).

JAHN, D., *et al.* 2018 Chemical-vapor deposited ultra-fast diamond detectors for temporal measurements of ion bunches. *Rev. Sci. Instrum*. **89** (9).

KIHARA, T., AONO, O., KIHARA, T. & AONO, O. 1963 Unified theory of relaxations in plasmas, I. Basic theorem. *J. Phys. Soc. Japan* **18** (6), 837–851.

KIM, I.J., *et al.* 2016 Radiation pressure acceleration of protons to 93 MeV with circularly polarized petawatt laser pulses. *Phys. Plasmas* **23** (7).

KROLL, F., *et al.* 2022 Tumour irradiation in mice with a laser-accelerated proton beam. *Nat. Phys*. **18** (3).

LI, C.K. & PETRASSO, R.D. 1993 Charged-particle stopping powers in inertial confinement fusion plasmas. *Phys. Rev. Lett*. **70** (20), 3059–3062.

MALKO, S., *et al.* 2021 Proton stopping measurements at low velocity in warm dense carbon. *Nat. Commun*. **13** (1), 1–12.

MAYNARD, G. & DEUTSCH, C. 1985 Born random phase approximation for ion stopping in an arbitrarily degenerate electron fluid. *J. Phys. Paris* **46** (7).

METTERNICH, M., *et al.* 2022 Analyzing the filamentation of MeV-range proton bunches in a laser-driven ion beamline and optimizing their peak intensity. *Phys. Rev. Accel. Beams* **25** (11).

PETER, T. & MEYER-TER-VEHN, J. 1991 Energy loss of heavy ions in dense plasma. II. Nonequilibrium charge states and stopping powers. *Phys. Rev.* A **43** (4), 2015–2030.

RAMIS, R., MEYER-TER VEHN, J. & RAMÍREZ, J. 2009 MULTI2D – a computer code for two-dimensional radiation hydrodynamics. *Comput. Phys. Commun*. **180** (6), 977–994.

RÖSCH, T.F., *et al.* 2020 A feasibility study of zebrafish embryo irradiation with laser-accelerated protons. *Rev. Sci. Instrum*. **91** (6).

ROTH, M., STÖCKL, C., SÜSS, W., IWASE, O., GERICKE, D.O., BOCK, R., HOFFMANN, D.H.H., GEISSEL, M. & SEELIG, W. 2000 Energy loss of heavy ions in laser-produced plasmas. *Europhys. Lett*. **50** (1), 28–34.

SCHMITZ, B., METTERNICH, M. & BOINE-FRANKENHEIM, O. 2022 Automated reconstruction of the initial distribution of laser accelerated ion beams from radiochromic film (RCF) stacks. *Rev. Sci. Instrum*. **93** (9).

TENG, J., GU, Y.Q., ZHU, B., HONG, W., ZHAO, Z.Q., ZHOU, W.M. & CAO, L.F. 2013 Beam collimation and energy spectrum compression of laser-accelerated proton beams using solenoid field and RF cavity. *Nucl. Instrum. Meth. Phys. Res. Sect.* A*: Accel. Spectrom. Detect. Assoc. Equip*. **729**, 399–403.

WAGNER, F., *et al.* 2016 Maximum proton energy above 85 MeV from the relativistic interaction of laser pulses with micrometer thick CH2 targets. *Phys. Rev. Lett*. **116** (20), 205002.

https://doi.org/10.1017/S0022377824000576 Published online by Cambridge University Press

WILKS, S.C., LANGDON, A.B., COWAN, T.E., ROTH, M., SINGH, M., HATCHETT, S., KEY, M.H., PENNINGTON, D., MACKINNON, A. & SNAVELY, R.A. 2001 Energetic proton generation in ultra-intense laser–solid interactions. *Phys. Plasmas* **8** (2), 542–549.

ZHU, J.G., *et al.* 2020 Demonstration of tailored energy deposition in a laser proton accelerator. *Phys. Rev. Accel. Beams* **23** (12).

ZIEGLER, J.F. & BIERSACK, J.P. 1985 The stopping and range of ions in matter. In *Treatise on Heavy-Ion Science*, pp. 93–129. Springer.

ZIEGLER, T., ASSENBAUM, S., BRACK, F.-E., COWAN, T.E., DOVER, N.P., KLUGE, T., KRAFT, S. & KROLL, F. 2023 Laser-driven high-energy proton beams from cascaded acceleration regimes. Research Square (submitted).

ZIMMERMAN, G.B. 1997 Monte Carlo methods in ICF. In *The 13th International Conference on Laser Interactions and Related Plasma Phenomena*, pp. 23–41. ASCE.

ZYLSTRA, A.B., 2015 Measurement of charged-particle stopping in warm dense plasma. *Phys. Rev. Lett.* **114** (21), 215002.

ZYLSTRA, A.B., RYGG, J.R., COLLINS, G.W., LI, C.K., FRENJE, J.A., PETRASSO, R.D., NAGEL, S.R., FITZSIMMONS, P. & REYNOLDS, H. 2020 Platform development for dE/dx measurements on short-pulse laser facilities. *High Energ. Dens. Phys.* **35** (2019).

https://doi.org/10.1017/S0022377824000576 Published online by Cambridge University Press